JOURNAL OF CATALYSIS 146, 62–68 (1994)

Structural Stability and Surface, Acidic, and Catalytic Properties of Magnesium Aluminophosphate of Type 36: Influence of Mg/P Ratios and of Thermal and Hydrothermal Treatments

Deepak Bansilal Akolekar[1]

Chemical Engineering Department, University of Laval, Ste-Foy, Quebec, Canada G1K 7P4

Received June 1, 1993; revised August 18, 1993

Effects of the thermal and hydrothermal treatments on the structural stability and physical properties (viz., surface concentrations of Mg, Al and P-, N_2-sorption capacity) of MAPO-36 have been studied. MAPO-36 has a higher thermal stability and a lower hydrothermal stability. MAPO-36 structure is thermally stable up to 823 K, and above the calcination temperature of 908 K, tridymite phase formation was observed. The partial conversion of MAPO-36 to amorphous material occurs due to the hydrothermal treatment at 398 K. The surface concentration of Mg decreases with the calcination temperature and also due to the hydrothermal treatment; however, the decrease is more significant with the latter. Changes in the lattice vibration region are observed due to the thermal and the hydrothermal treatments. *In situ* IR spectroscopic investigations of chemisorbed pyridine on the MAPO-36 catalysts revealed that the concentration of Brønsted and Lewis acid sites are strongly affected by the Mg-content in the $AlPO_4$-36 framework, thermal and hydrothermal treatments. The ratio of Brønsted to Lewis acid sites decreases with the decrease in the concentration of framework-substituted Mg and also by the thermal and hydrothermal treatments. MAPO-36 materials with different Mg-content and the hydrothermally treated MAPO-36 possesses a broad array of acid strength distributions. The number of weak and strong acid sites are influenced by the concentration of framework-substituted Mg in the $AlPO_4$-36 and by the thermal and the hydrothermal treatments. The catalytic activities of MAPO-36 (with different Mg/P ratios) and the thermally and hydrothermally treated MAPO-36 catalysts in *n*-hexane, isooctane, and toluene conversion reactions were studied. In *n*-hexane and isooctane reactions, the conversion and the aromatic formation decrease with the decrease in the Mg-content in the AlPO-36 framework. This is in agreement with the increase in the strong acid sites with framework Mg-concentration. The thermal treatment causes a pronounced decrease in the catalytic activity of MAPO-36 in these reactions than does the hydrothermal treatment. The aliphatic and aromatic distributions are different in these reactions over the MAPO-36 materials. The toluene disproportionation activity of the MAPO-36 is affected by the Mg-content and the thermal and hydrothermal treatments.

INTRODUCTION

The magnesium aluminophosphate of type 36 (MAPO-36) molecular sieve reported by Flanigen *et al.* (1) has a unique three-dimensional structure with monoclinic symmetry and cell parameters a = 13.148 Å, b = 21.577 Å, c = 5.164 Å, and β = 91.84°. MAPO-36 has the 4.6.12 two-dimensional net similar with annular side pockets (unlike cancrinite). The channels are elliptical (10.1 by 9.2 Å across in projection), parallel to the c-axis, and have a pore opening of 7.4 by 6.5 Å (2, 3). In our earlier investigations (4–6), the preparation, characterization, acidity and site energy distribution of MAPO-36 are already reported. MAPO-36 contains both Brønsted and Lewis acid sites (1, 5). MAPO-36 shows considerable catalytic activity in linear- (7), branched-, and cycloalkanes, aromatic hydrocarbons, and the alcohol-to-aromatics conversion reactions (6). In the present study, the thermal and hydrothermal structural stability of MAPO-36 and the influence of the magnesium content (Mg/P ratios) and the thermal and hydrothermal treatments on the N_2-sorption capacity, surface composition, acidity, and catalytic properties of the magnesium aluminophosphate of type 36 are investigated.

EXPERIMENTAL

Pr_3N–MAPO-36 catalysts were synthesized by the hydrothermal procedures reported earlier (4, 7). Pr_3N–MAPO-36 materials with different Mg-content designated as Pr_3N–MAPO-36[A], Pr_3N–MAPO-36[B], and Pr_3N–MAPO-36[C] were obtained by crystallizing the respective gel of composition {Pr_3N–MAPO-36[A]: 1.8 Pr_3N · 0.176 MgO · 0.912 Al_2O_3 · 1.00 P_2O_5 · 40 H_2O · 0.34 HOAc; Pr_3N–MAPO-36[B]: 1.8 Pr_3N · 0.142 MgO · 0.931 Al_2O_3 · 1.01 P_2O_5 · 40 H_2O · 0.28 HOAc; and Pr_3N–MAPO-

[1] Please address reprint requests to the author at the Department of Physical Chemistry, The University of New South Wales, P.O. Box 1, Kensington, NSW 2033, Australia.

0021-9517/94 $6.00

36[C]: 1.8 Pr_3N · 0.112 MgO · 0.945 Al_2O_3 · 1.01 P_2O_5 · 40 H_2O · 0.22 HOAc} initially at 378 K for 50 h and further at 423 K for 24 h in a teflon-coated autoclave. The MAPO-36 crystallization was carried out without stirring. The crystals of the magnesium aluminophosphate were washed thoroughly with deionised water, filtered, and dried in an air oven at 373 K for 16 h. The organic template was removed by calcination in the presence of air at 823 K for 18 h. The details of preparation and characterization of the MAPO-36 catalyst are given elsewhere (4).

The procedures used for the thermal and hydrothermal treatment of MAPO-36 are as follows. *Thermal treatment:* MAPO-36[A] (3 g) was calcined at different temperatures in the range 823–1173 K for 18 h in an muffle furnace. *Hydrothermal treatment:* MAPO-36[A] (3 g) particles were placed in a stainless-steel wire mesh basket and suspended in a stainless-steel pressure bomb containing water at the bottom. The distance between the wire mesh basket and water level was maintained so that the material is only in contact with water vapours. The closed bomb was then heated in an air oven at 398 K for 72 h. The hydrothermally treated material was dried in an vacuum oven at 373 K for 16 h and then calcined at 823 K for 5 h.

The synthesized materials and the thermally and hydrothermally treated materials were characterized as follows: The X-ray powder diffraction spectra were obtained by a Holland Philips PW/1730 X-ray generator with an Ni-filtered Cu$K\alpha$ radiation source and a scintillation counter. Atmoic absorption spectroscopy and gravimetric and C, H, N analysis were used for elemental analysis. The N_2-sorption capacity data of the materials were obtained by N_2 adsorption/desorption technique (p/p_0 = 0.3) using a Quantasorb unit (Quantachrome Corp., U.S.A.). XPS measurements were conducted for determining the surface concentration and binding energy of O_{1s}, Mg_{2p}, Al_{2p}, and P_{2p}. A V.G. Scientific Escalab Mark II system with a hemispherical analyzer operated in the constant pass energy mode (20 eV) was employed. An Mg$K\alpha$ X-ray source ($h\nu$ = 1253.6 eV) was operated at 20 mA and 15 kV. The intensity of XPS band was determined using linear background subtraction and integration of peak areas. IR spectra of the untreated and treated MAPO-36 materials in the lattice vibration range (1250–400 cm^{-1}) were obtained with 2 cm^{-1} resolution using a Digilab-FTS-60 spectrometer. The procedures for the *in situ* IR acidity, the strong acid sites and the site energy distribution measurements were reported earlier (4, 8, 9).

The catalytic activities of the catalysts in *n*-hexane, isooctane, and toluene conversion reactions were determined in a pulse microreactor (i.d. 4mm) connected to a gas chromatograph. The reaction conditions are mentioned in the respective tables. Before the activity was measured, the catalyst was heated at 673 K for 1 h in a flow of helium. The details of the microreactor, the product analysis conditions, and the procedure of measuring the activity of the catalyst are given elsewhere (9).

RESULTS AND DISCUSSION

Thermal and Hydrothermal Stability of MAPO-36

The properties of MAPO-36 materials are presented in Table 1. The crystallinity (obtained from XRD data) and N_2-sorption capacity measurements show the high crystalline nature of the MAPO-36[A–C] materials. The data (Table 1) indicated that the increase in the calcination temperature of MAPO-36[A] from 823 to 1173 K results a significant decrease in its crystallinity and N_2-sorption capacity. At the calcination temperature of 873 K, the crystallinity and N_2-sorption capacity of MAPO-36[A] were decreased by 19 and 26%, respectively. The formation of tridymite phase was observed at the calcination temperature of 908 K. The amount of tridymite phase formed at this calcination temperature was 30%. The extent of tridymite formation increases with the calcination temperature. The decrease in the crystallinity and N_2-sorption capacity of MAPO-36[A] is more pronounced in the calcination temperature range of 873–973 K. The results lead to the conclusion that unlike zeolites (9) and $AlPO_4$-5 (10), MAPO-36 has a low thermal stability. The decrease in the crystallinity (by 77%) and N_2-sorption capacity (by 78%) of MAPO-36[A] was observed after the hydrothermal treatment. The hydrothermal treatment causes the partial degradation of MAPO-36[A] to amorphous material (67%). This shows that MAPO-36 has very poor hydrothermal stability compared with ZSM-5 zeolite (11).

Composition of MAPO-36

The surface and bulk composition of the thermally and hydrothermally treated MAPO-36[A] are presented in Table 2. Examination of the bulk and surface composition results of the thermally treated MAPO-36[A] revealed that the concentration of magnesium is higher on the surface than in the bulk. The surface concentration of magnesium decreases with the calcination temperature. It seems thus that the structural collapse associated with increasingly higher calcination temperature is accompanied by Mg-extraction from the $AlPO_4$-36 framework. The concentration of phosphorus increases on the surface with the calcination temperature above 823 K. The trend is reversed for the surface concentration of Al. The hydrothermal treatment drastically affects the surface composition of MAPO-36[A] (Table 2). The Mg-concentration is decreased by 60% on the surface of the hydrothermally treated MAPO-36[A3]. The higher Al/P ratio on the surface of MAPO-36[A3] indicates that the concentration of aluminium increases on the surface after the hydrothermal treatment. The increase in the Al-concentration is due to

TABLE 1

Properties of Magnesium Aluminophosphate (Type 36) Catalysts

Catalyst	Molar chemical composition	Calcination temperature (K)	Crystalline phases(s)	Crystallinity (%)[c]	N_2-sorption Capacity (mmol · g^{-1})	Strong acid sites q_i(673 K) (μmol · g^{-1})
MAPO-36[A]	0.18 MgO · 0.911 Al_2O_3 · 1.0 P_2O_5	823	MAPO-36	100	5.60	43.5
MAPO-36[B]	0.14 MgO · 0.930 Al_2O_3 · 1.0 P_2O_5	823	MAPO-36	100	5.45	34.6
MAPO-36[C]	0.11 MgO · 0.945 Al_2O_3 · 1.0 P_2O_5	823	MAPO-36	98	5.41	25.0
MAPO-36[A1][a]	0.18 MgO · 0.911 Al_2O_3 · 1.0 P_2O_5	973	MAPO-36 Tridymite (77%)	23	0.30	<0.5
MAPO-36[A2][a]	0.18 MgO · 0.911 Al_2O_3 · 1.0 P_2O_5	1173	MAPO-36 Tridymite (90%)	10	0.15	—
MAPO-36[A3][b]	0.18 MgO · 0.911 Al_2O_3 · 1.0 P_2O_5	823	MAPO-36 Amorph. (67%)	33	1.24	8.0

Note. Amorph., amorphous phase.
[a] Thermally treated.
[b] Hydrothermally treated.
[c] Crystallinity of MAPO-36 phase.

the hydrolysis of framework Al and the structural collapse of MAPO-36[A].

Infrared Examination of MAPO-36

Changes in the lattice vibration region (1200–400 cm^{-1}) of the uncalcined, thermally and hydrothermally treated MAPO-36[A] materials are shown in Fig. 1. The bands between 1000 and 1200 cm^{-1} are assigned to the asymmetric stretch of TO_4 tetrahedra and these are characteristic of all zeolites and zeolite-like materials (12). The absorption in the region 500–600 cm^{-1} has been assigned to vibrations in the double ring region. Other bands in the spectra of Pr_3N–MAPO-36[A]/MAPO-36[A] between 650 and 750 cm^{-1} and between 450 and 490 cm^{-1} are assigned to symmetric stretches and to the T–O bend, respectively. After the thermal and hydrothermal treatments of MAPO-36[A], the bands in the region 400–1200 cm^{-1} are shifted to higher frequency. In the thermally treated MAPO-36[A1] and MAPO-36[A2], additional bands at 626, 713, and 730 cm^{-1} are observed. Comparison of the lattice vibration region of MAPO-36[A], MAPO-36[A1], and MAPO-36[A3] indicatesc that the changes in the lattice have occurred due to the thermal treatments at the elevated temperatures. The higher temperature treatments causes structural collapse and transformations to the tridymite and amorphous phases. The IR spectrum of the hydrothermally treated MAPO-36[A3] in the lattice vibration region is similar to that of MAPO-36[A], which is consistent with the decrease in the crystallinity and the formation of amorphous material during the hydrothermal treatment.

IR spectra after the desorption of pyridine at 463 K from the MAPO-36 catalysts are shown in Fig. 2. The bands at 1447 and 1545 cm^{-1} ascribed to Lewis and Brønsted acid sites, respectively, are close to their usual values (13). The results of the changes in the absorbance

TABLE 2

Surface and Bulk Composition of the Untreated and Thermally and Hydrothermally Treated MAPO-36[A] Catalysts

	Surface concentration (Atomic%)				Atomic ratio			
					Mg/P		Al/P	
Catalyst	Al_{2p}	Mg_{2p}	P_{2p}	O_{1s}	Surface	Bulk	Surface	Bulk
MAPO-36[A]	16.0	3.6	18.0	62.4	0.200	0.080	0.920	0.915
MAPO-36[A1]	15.1	3.0	17.6	64.3	0.172	0.085	0.888	0.915
MAPO-36[A2]	15.4	1.9	17.9	64.8	0.110	0.085	0.855	0.915
MAPO-36[A3]	18.2	1.4	16.0	64.4	0.086	0.085	1.139	0.195

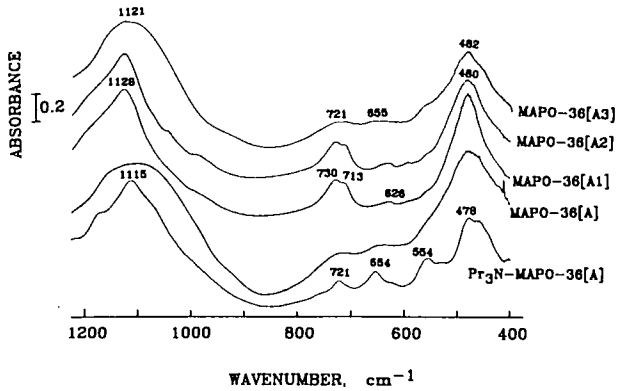

FIG. 1. Mid-FTIR spectra of Pr_3N–MAPO-36[A], MAPO-36[A], MAPO-36[A1], MAPO-36[A2], and MAPO-36[A3].

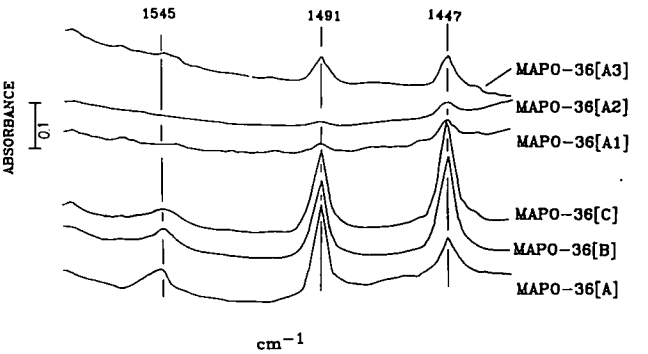

FIG. 2. *In situ* infrared spectra of chemisorbed pyridine on the magnesium aluminophosphate of type-36 catalysts (pyridine chemisorbed at 463 K).

(1447 and 1545 cm^{-1}) for the catalysts (Table 3) indicate that the concentration of Brønsted and Lewis acid sites are affected by the framework Mg-content and the thermal and hydrothermal treatments. The concentration of Brønsted acid sites and the ratio of Brønsted to Lewis acid sites decreases with the decrease in Mg-content in the aluminophosphate framework and by the thermal and hydrothermal treatments. Further, the decrease in the concentration of Lewis acid sites is also observed with the Mg-content in the aluminophosphate and with the calcination temperature. The high-temperature treatment (>973 K) of MAPO-36[A] causes the structural collapse, owing to its low structural stability at the elevated temperatures. Thus, markedly affecting the concentrations of Lewis and Brønsted acid sites. The concentration of Brønsted and Lewis acid sites on MAPO-36[A3] is lower than that on MAPO-36[A], which is due to the partial transformation (67%) of the crystalline material to amorphous material during the hydrothermal treatment. The order of the density of Brønsted acid sites over the catalysts is as follows: MAPO-36[A] > MAPO-36[B] > MAPO-36[C] >>> MAPO-36[A3] >>>> MAPO-36[A1] and MAPO-36[A2].

TABLE 3

Data on Brønsted and Lewis Acid Sites of Magnesium Aluminophosphate (Type 36) Catalysts

Catalyst	Absorbance of pyridine (A.U.)		
	Brønsted acid sites (B)	Lewis acid sites (L)	B/L
MAPO-36[A]	0.29	0.37	0.78
MAPO-36[B]	0.20	0.40	0.49
MAPO-36[C]	0.09	0.52	0.39
MAPO-36[A1]	—	0.06	—
MAPO-36[A2]	—	0.03	—
MAPO-36[A3]	0.01	0.09	0.11

Site Energy Distributions and Strong Acid Site Results for MAPO-36

The site energy distribution obtained from the stepwise thermal desorption (STD) of pyridine on MAPO-36[A–C] and MAPO-36[A3] are shown in Fig. 3. The strength of the site involved in the pyridine chemisorption is expressed in terms of the desorption temperature (T_d), which lies in the range of temperature in which the chemisorbed pyridine is desorbed. Here, T_d^* is the measure of the maximum strength possessed by the site and corresponds to the temperature at which the pyridine chemisorbed on the strongest sites is desorbed. The columns in the figure show the strength distribution of the sites (equivalent to 0.10 mmol · g^{-1} {for MAPO-36[A]}, 0.24 mmol · g^{-1} {for MAPO-36[B]}, 0.156 mmol · g^{-1} {for MAPO-36[C]}, and 0.045 mmol · g^{-1} {for MAPO-36[A3]}) involved in the

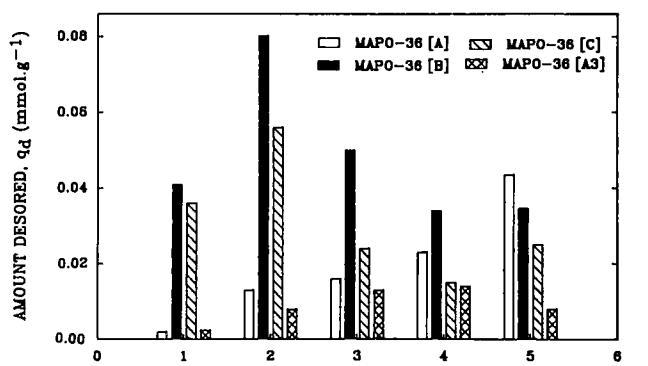

FIG. 3. Site energy distribution on MAPO-36[A], MAPO-36[B], MAPO-36[C], and MAPO-36[A3]: (1) 323 K < T_d < 373 K; (2) 373 K < T_d < 473 K; (3) 473 K < T_d < 573 K; (4) 573 K < T_d < 673 K; (5) 673 K < $T_d \leq T_d^*$.

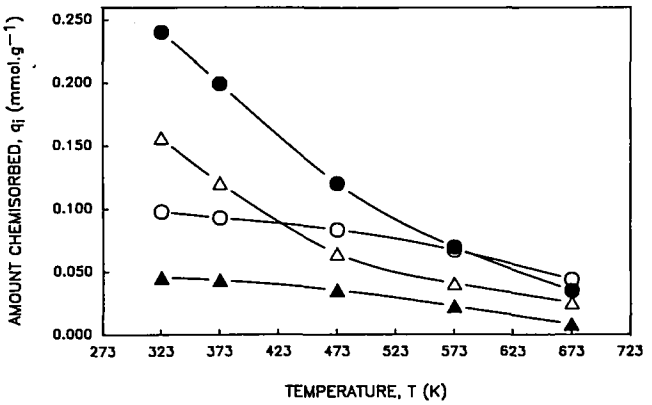

FIG. 4. Temperature dependence of the chemisorption of pyridine on: ○, MAPO-36[A]; ●, MAPO-36[B]; △, MAPO-36[C]; and ▲, MAPO-36[A3].

chemisorption at the lowest temperature of the STD (i.e., 323 K). The sites of strength 673 K $< T_d \leq T_d^*$ were obtained from the amount of pyridine chemisorbed at 673 K. On the other hand, the number of sites of strength $T_1 < T_d \leq T_2$ was obtained from the amount of pyridine which was initially chemisorbed at T_1 but desorbed by increasing the temperature to T_2. Figure 4 shows the temperature dependence of the chemisorption of pyridine on MAPO-36[A–C] and MAPO-36[A3] obtained from the STD data. The chemisorption of pyridine at higher temperatures points to the involvement of the stronger sites. The q_i vs T curve, therefore, presents a type of site energy distribution in which the number of sites is expressed in terms of the amount of pyridine chemisorbed as a function of the desorption temperature.

The results of the STD of pyridine have clearly shown that a broad site energy distribution exists on the MAPO-36 catalysts containing the different concentration of magnesium. The distribution of weak and strong acid sites are affected by the Mg content in the $AlPO_4$-36 framework and the hydrothermal treatment. MAPO-36[B] and MAPO-36[C] (both containing lower Mg content than MAPO-36[A]) possesses a greater number of weak acid sites than MAPO-36[A]. The number of strong acid sites (measured in terms of the chemisorption of pyridine at 673 K) (Table 1) on the magnesium aluminophosphate catalysts is strongly influenced by the Mg-content and thermal and hydrothermal treatments. The order of the strong acid sites follows the order of the density of Brønsted acid sites over the catalysts. The changes in the acid strength distribution and the decrease in the number of strong acid sites over the thermally and hydrothermally treated MAPO-36 are caused by the partial/complete structural collapse of MAPO-36 during the respective treatments.

Catalytic Activity of MAPO-36

The influence of Mg/P ratios and thermal and hydrothermal treatments on the catalytic activity and aromatic selectivity of MAPO-36 catalysts in *n*-hexane, isooctane, and toluene conversion reactions are presented in Tables 4 and 5. The catalytic activity and aromatic selectivity

TABLE 4

Conversion of *n*-Hexane over Magnesium Aluminophosphate (Type 36) Catalysts

Catalyst	MAPO-36[A]	MAPO-36[B]	MAPO-36[C]	MAPO-36[A1]	MAPO-36[A2]	MAPO-36[A3]
Conversion (%)	90.0	79.5	65.6	0.6	<0.1	43.2
Aromatic concentration (wt%)	25.2	16.8	7.8	—	—	2.3
Product distribution (wt%)						
CH_4	2.8	1.2	0.3			0.1
C_2-aliphatics	25.6	35.1	36.4			38.0
C_3-aliphatics	16.0	18.2	25.0			28.0
C_4-aliphatics	12.5	18.3	23.9			26.5
C_{5+}-aliphatics	15.1	6.1	2.6			2.1
Aromatics	28.0	21.1	11.8			5.3
Total	100	100	100			100
Aromatics distribution (wt%)						
Benzene	1.6	2.3	4.9			8.7
Toluene	9.5	13.2	26.2			30.4
Ethylbenzene	—	0.4	1.6			—
Xylenes	26.2	34.5	42.7			34.8
Trimethylbenzenes	19.4	15.1	9.8			8.7
Other C_{9+}-aromatics	43.3	34.5	14.8			17.4
Total	100	100	100			100

Note. Reaction conditions: Amount of catalyst, 0.100 g; He flow rate, 30 cm^3 · min^{-1}; pulse size, 1 μl; temperature, 673 K.

TABLE 5

Conversion of Isooctane over Magnesium Aluminophosphate (Type 36) Catalysts

Catalyst	MAPO-36[A]	MAPO-36[B]	MAPO-36[C]	MAPO-36[A1]	MAPO-36[A2]	MAPO-36[A3]
Conversion (%)	74.4	66.1	58.4	1.1	<0.4	56.4
Aromatic concentration (wt%)	16.5	11.5	8.4	<0.1		4.5
Product distribution (wt%)						
CH_4	1.8	0.7	0.1			0.3
C_2-aliphatics	22.0	19.5	18.0			33.2
C_3-aliphatics	27.0	40.6	64.7			34.4
C_4-aliphatics	13.0	16.5	8.3			21.0
C_{5+}-aliphatics	14.0	5.3	0.5			3.3
Aromatics	22.2	17.4	8.4			8.0
Total	100	100	100			100
Aromatics distribution (wt%)						
Benzene	3.6	2.5	4.8			4.4
Toluene	16.3	12.8	35.7			8.9
Ethylbenzene	—	—	1.2			—
Xylenes	35.2	32.8	25.0			31.1
Trimethylbenzenes	17.6	21.9	7.1			8.9
Other C_{9+}-aromatics	27.3	30.0	26.2			46.7
Total	100	100	100			100

Note. Reaction conditions: amount of catalyst, 0.100 g; He flow rate, 30 $cm^3 \cdot min^{-1}$ pulse size, 5 μl; temperature, 673 K.

increases with the Mg content in the $AlPO_4$-36 framework. Current acidity investigations on the MAPO-36 catalysts revealed that the number of strong acid sites, and the density of Brønsted acid sites are increased with the Mg content in the $AlPO_4$-36 framework. MAPO-36[A] possesses a greater number of strong acid sites among the catalysts. The thermally treated MAPO-36[A1] and MAPO-36[A2] showed lower *n*-hexane and isooctane conversion than MAPO-36[A]. The large decrease in the catalytic activities of the thermally treated MAPO-36 catalysts is consistent with the presence of very few acid sites. The hydrothermally treated MAPO-36[A3] showed higher catalytic activity and aromatics formation than the thermally treated MAPO-36[A1, A2] catalysts but lower than MAPO-36[A]. The results of *in situ* IR acidity measurements and the STD of pyridine showed that the number of strong acid sites is decreased after the hydrothermal treatment. Further the number of strong acid sites on the hydrothermally treated MAPO-36[A3] are more than that on the thermally treated MAPO-36[A1, A2] catalysts. The aliphatic and aromatic distribution in *n*-hexane and isooctane conversion reactions over the magnesium aluminophosphate catalysts are different. The formation of C_2- and C_3-aliphatics decreases and that of the C_5-aliphatics and aromatics increases with the Mg content in the catalysts.

TABLE 6

Product Distribution in Toluene Disproportionation over Magnesium Aluminophosphate (Type 36) Catalysts

Catalyst	MAPO-36[A]	MAPO-36[B]	MAPO-36[C]	MAPO-36[A1]	MAPO-36[A2]	MAPO-36[A3]
Conversion (%)	52.4	40.1	32.3	1.3	<0.6	19.7
Product distribution [Hydrocarbons (wt%)]						
Aliphatics	1.5	1.8	0.4	0.1		2.0
Benzene	23.5	16.0	12.0	0.2		8.3
Toluene	47.6	59.9	67.7	98.7		80.3
p-Xylene	7.5	5.9	4.5	0.1		2.0
m-Xylene	9.0	7.2	6.6	0.2		3.8
o-Xylene	5.1	6.6	5.3	0.1		3.2
C_{9+}-aromatics	5.3	2.6	3.5	0.6		0.4
Total	100	100	100	100		100

Note. Reaction conditions: amount of catalyst, 0.100 g; He flow rate, 30 $cm^3 \cdot min^{-1}$, pulse size, 1 μl; temperature, 673 K.

The product distribution in toluene disproportionation on the magnesium aluminophosphate catalysts at 673 K are given in Table 6. MAPO-36[A] exhibited higher catalytic activity and the formation of more benzene, xylenes, and C_{9+}-aromatics than MAPO-36[B], MAPO-36[C], and the thermally and hydrothermally treated MAPO-36[A] catalysts. The high toluene disproportionation activity of MAPO-36[A] as compared with the other untreated and treated MAPO-36 catalysts is due to the presence of a higher number of strong acid sites.

CONCLUSIONS

Calcination of MAPO-36 at higher temperatures (>823 K) results in a decrease in the crystallinity and N_2-sorption capacity. Above the calcination temperature of 908 K, a phase transformation to tridymite was observed. The extent of phase transformation to tridymite increase with the calcination temperature. The hydrothermal treatment causes a significant decrease in the crystallinity and MAPO-36. The results of bulk and surface composition indicate that the concentration of Mg, Al, and P on the surface of MAPO-36 are strongly affected by the thermal and hydrothermal treatments.

The Mg-content in the $AlPO_4$-36 framework and the thermal and hydrothermal treatments, all show a strong influence on the concentration of Brønsted and Lewis acid sites, the ratio of Brønsted to Lewis acid sites, strong acid sites, and acid strength distribution of the magnesium aluminophosphate of type-36 catalysts.

The catalytic properties of the magnesium aluminophosphate of type-36 catalysts are also significantly affected by the Mg/P ratios in the MAPO-36 and by the thermal and hydrothermal treatments.

ACKNOWLEDGMENTS

The author is sincerely thankful to Dr. H. G. Karge, Fritz Haber Institute of the Max Planck Society, Berlin, Germany, for providing the experimental facilities and helpful discussions. The author is grateful to the Alexander von Humboldt Foundation, Bonn, Germany, for the award of an international research fellowship.

REFERENCES

1. Flanigen, E. M., Lok, B. M., Patton, R. L., and Wilson, S. T., *in* "Proceedings, 7th International Zeolite Conference, Tokyo, 1986" (Y. Murakami, A. Iijima, and J. W. Ward, Eds.), p. 103. Kodansha, Tokyo 1986.
2. Smith, J. V., Pluth, J. J., and Andries, K. J., *in* "Atlas of Zeolite Structure Types" (W. M. Meir and D. H. Olson, Eds.), 3rd revised ed., p. 50. Butterworth–Heinemann, London, 1992.
3. Smith, J. V., Pluth, J. J., and Andries, K. J., *Zeolites* **13** (3), 166 (1993).
4. Akolekar, D. B., *J. Catal.* **143,** 227 (1993).
5. Akolekar, D. B., *Zeolites,* (1993) in press.
6. Akolekar, D. B., *J. Catal.* **144,** 148 (1993).
7. Wilson, S. T., and Flanigen, E. M., *ACS Symp. Ser.* **398,** 329 (1989).
8. Akolekar, D. B., and Kaliaguine, S. K., *J. Chem. Soc. Faraday Trans.*, in press.
9. Akolekar, D. B., "Sorption, Diffusion and Catalytic Reactions on Zeolites and Zeolite-like Materials." Ph.D. thesis, University of Poona, Poona, 1987.
10. Choudhary, V. R., Akolekar, D. B., Singh, A. P., and Sansare, S. D., *J. Catal.* **111,** 254 (1988).
11. Nayak, V. S., and Choudhary, V. R., *Appl. Catal.* **10,** 137 (1984).
12. Flanigen, E. M., *in* "Zeolite Chemistry and Catalysis" (J. A. Rabo, Ed.), Vol. 171, p. 80. ACS Monograph, Washington, DC, 1976.
13. Ward, J. W., *in* "Zeolite Chemistry and Catalysis" (J. A. Rabo, Ed.), Vol. 171, p. 118. ACS Monograph, Washington, DC, 1976.